Supplementary Information for

Organic-inorganic perovskite plasmonic nanowire lasers with low thresholds and good thermal stability

Haichao Yu,[a, c] Kuankuan Ren,[b] Qiang Wu,[d] Jian Wang,[a] Jie Lin,[a] Zhijie Wang,[b] Jingjun Xu,[d] Rupert F. Oulton,[c] Shengchun Qu[b] and Peng Jin[a]

[a]Research Center of Ultra-Precision Optoelectronic Instrument, Harbin Institute of Technology, Harbin 150080, China.

[b]Key Laboratory of Semiconductor Materials Science, Institute of Semiconductors, Chinese Academy of Sciences, Beijing 100083, China.

[c]The Blackett Laboratory, Imperial College London, London SW7 2AZ, United Kingdom.

[d]The MOE Key Laboratory of Weak Light Nonlinear Photonics, Nankai University, Tianjin 300457, China

1. Numerical calculations of guided modes in the nanowire cavities

The cross-section waveguide-mode properties (effective indices and field distributions) of the $CH_3NH_3PbI_3$ nanowire/MgF_2/Ag hybrid plasmonic configuration and the $CH_3NH_3PbI_3$ nanowire/SiO_2 photonic configuration were calculated using finite-element method (COMSOL). The wavelength was set at 790 nm. The (n, k) value of $CH_3NH_3PbI_3$ at 790 nm were set to be (n = 2.3, k =0.15).[1]

Fig. S1(a) and S1(b) show the confinement factor and the propagation length as a function of the $CH_3NH_3PbI_3$ width with different MgF_2 spacer thicknesses. Thinner spacer can provide stronger mode confinement, however, the loss increases as the spacer thickness decreases. In our experiment, we choose the 10 nm as the MgF_2 thickness, as this thickness can provide good optical confinement with acceptable loss as well as allow continuous film deposition.

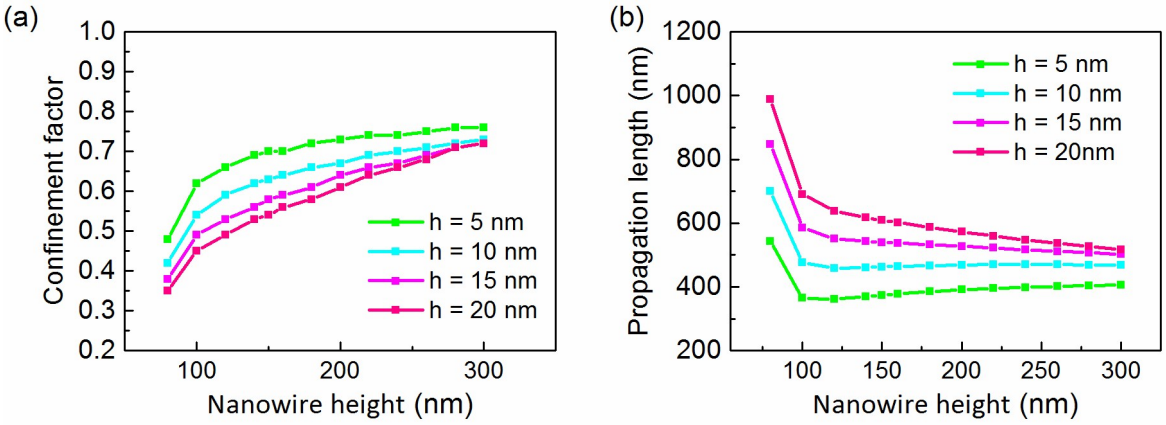

Fig. S1. The mode confinement factor (a) and propagation length (b) for different MgF_2 thickness

Fig. S2 shows the effective indices of fundamental mode against the nanowire height (aspect ratio = 1 and 2), as a supplementary for Fig. 1c in the main text. For the photonic configuration, the nanowire is directly put on SiO_2(n_{SiO2} = 1.454), only fundamental TE modes are shown here, we can see it experiences a cut-off at around 400 nm, 225 nm, on the contrary, the plasmonic mode can still exist when the height is as small as 50 nm.

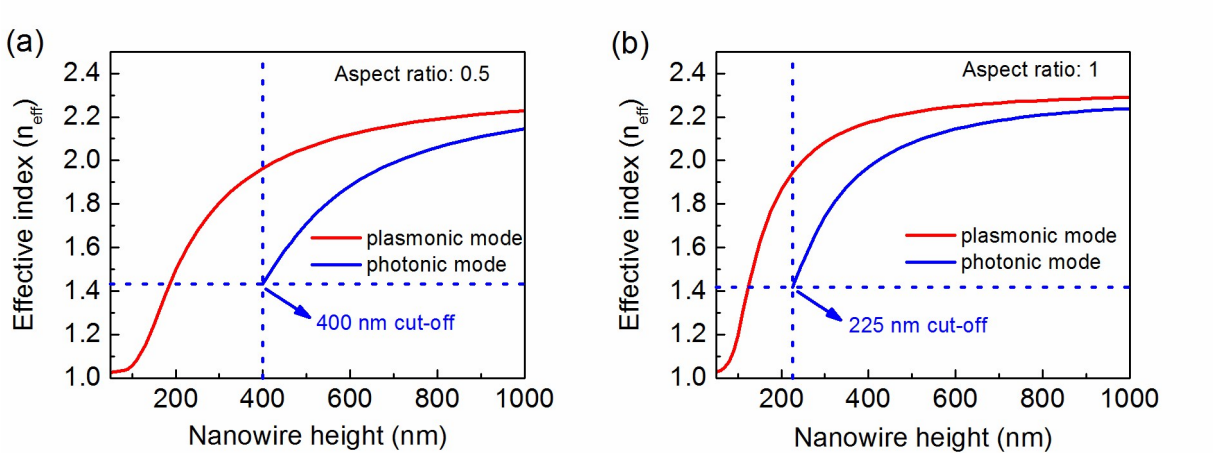

Fig. S2. Calculated effective mode indices against nanowire height for photonic and plasmonic lasing geometries with three different aspect ratios: (a) 0.5, (b) 1

2. Synthesis of single crystal perovskite $CH_3NH_3PbI_3$ nanowires

Lead acetate trihydrate ($PbAc_2 \cdot 3H_2O$, 99%) was obtained from Beijing Chemical Reagent Company. Methylammonium iodide (CH_3NH_3I, 99.5%) was purchased from Xi'an Polymer Light Technology Corp. Ethyleneglycol monomethyl ether ($CH_3OCH_2CH_2OH$, 98%) was purchased from Xilong Chemical CO.LTD. Isopropanol (IPA, C_3H_8O, 99.7%) was purchased from Tianjin Fengchuan Chemical Reagent Co. LTD. Poly (3, 4-ethylenedioxythiophene) polystyrene sulfonate (PEDOT: PSS, Clevios PVP. AI 4083) was purchased from Heraeus. Glass substrates were supplied from Zhuhai Kaivo Optoelectronic Tech. Co. LTD, China.

All chemicals were used as received without further purification. The synthesis process is shown in Fig. S3. A glass substrate was washed with deionized water under ultrasonic environment and cleaned by ultraviolet ozone. A buffer layer of high hydrophilous PEDOT: PSS thin film was spin-coated onto the substrate at 3000 rpm for 40 seconds before it was annealed at 150 ^oC for 15 minutes, then the temperature dropped to 65 ^oC naturally within 15 minutes. Afterwards, the substrate was drop-cast with several tens of microliters of unsaturated ethylene glycol monomethyl ether solution of lead acetate trihydrate, which spread easily along the PEDOT: PSS layer. The sample was annealed at 65 ^oC for 30 minutes

in air. After the sample was cooled, the substrate was carefully faced down or faced up in a CH_3NH_3I/IPA (1mL) solution with a concentration of 40 mg/mL at room temperature. The surface color of the sample turned to be light brown rapidly, due to the formation of a crystalline $CH_3NH_3PbI_3$ thin layer on the surface. After several hours, the brown films turned black. The reaction was then allowed to proceed for 16 to 20 hours to form $CH_3NH_3PbI_3$ nanowires. In the end, the $CH_3NH_3PbI_3$ nanowires were gently washed in isopropanol and dried under a stream of nitrogen flow.

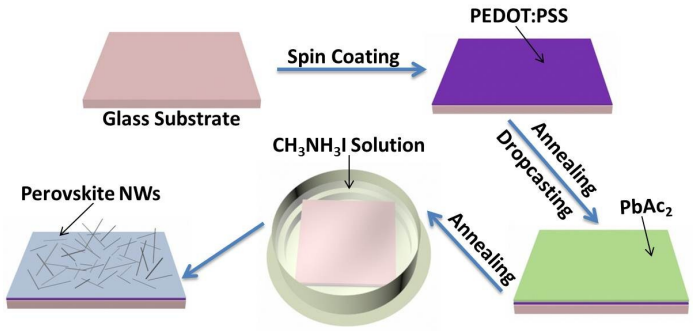

Fig. S3. Schematic of the synthesis process of the perovskite nanowires.

3. Structural characterizations of $CH_3NH_3PbI_3$ nanowires

The PXRD data of the nanowires were acquired on a Rigaku SmartLab diffractometer in the 2-theta range of 10°-60° with an interval of 0.02°. The scanning electron microscope (SEM) images were collected on a Zeiss Sigma field-emission SEM operated at 3 kV. Some selected SEM images are shown in Fig. S4. The typical nanowires present lengths about 4-8 μm and widths around 200-500 nm. The nanowires investigated here have cross-sectional aspect ratio typically around 1-2. The nanowires sample for transmission electron microscope (TEM) was dry-transferred and dispersed onto a copper grid. The TEM images were acquired on a JEM-2010 (Japanese electronic optical co, LTD) TEM at an operating voltage of 120 kV. Energy-dispersive X-ray spectroscopy (EDS) was also performed from this integrated TEM equipped with an Oxford Inca EDS with an I/Pb ratio of 2.76, which is consistent with the $CH_3NH_3PbI_3$ stoichiometry (Fig. S5).

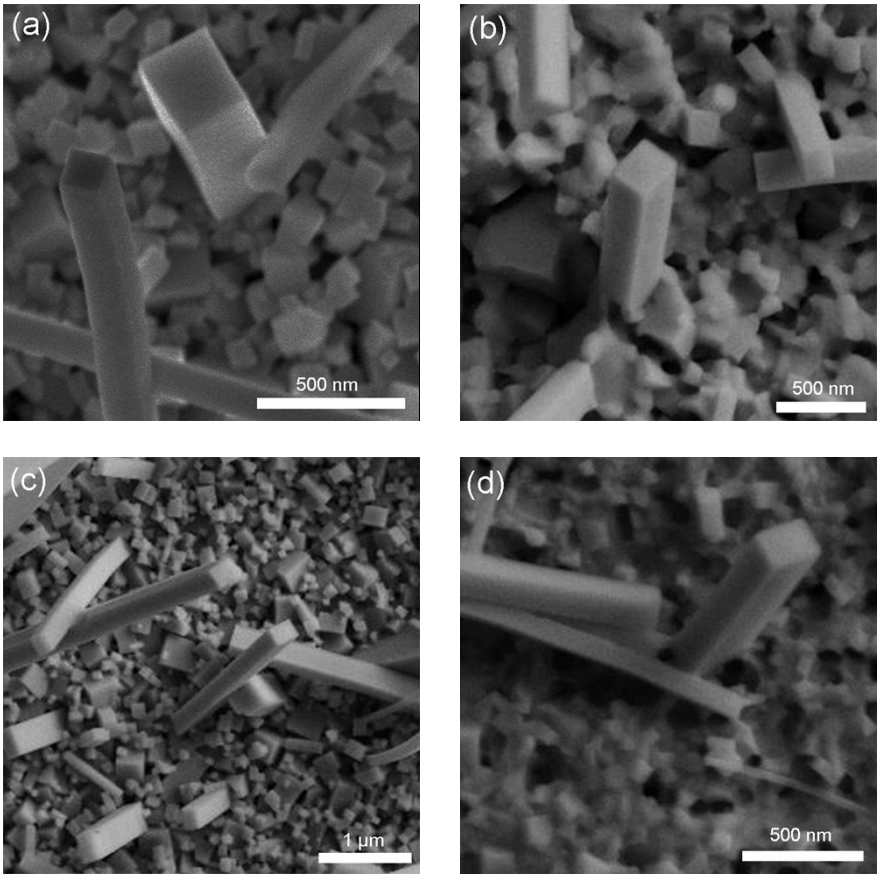

Fig. S4. SEM images of $CH_3NH_3PbI_3$ nanowires. The synthesized nanowires show flat rectangular end facets.

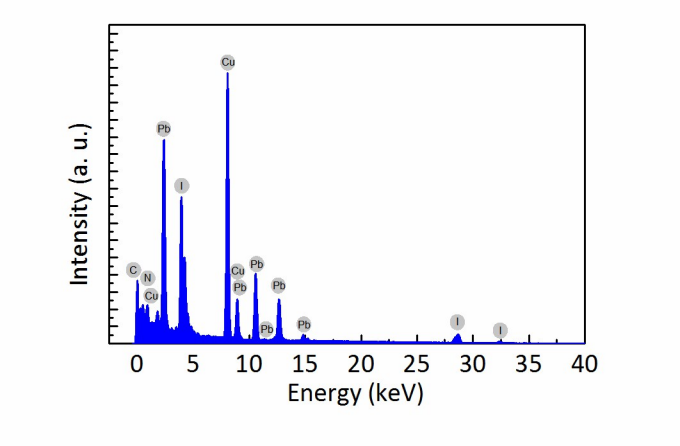

Fig. S5. A representative EDS spectrum of a single $CH_3NH_3PbI_3$ nanowire on a copper grid.

4. Optical characterization of $CH_3NH_3PbI_3$ nanowires

Steady-state Photoluminescence (PL) spectra were conducted at room temperature on Cary Eclipse Fluorescence(Varian) with an excitation wavelength of 450 nm. The absorption spectra of nanowires were conducted at room temperature on a double beam ultra violet (UV) spectrophotometer of TU1950 (Beijing Purkinje General Instrument Co, LTD). The PL and optical absorption spectra of the as-grown perovskite nanowires are shown in Fig. S6. Analysis of the sharp absorption onset shows a low concentration of in-gap defects. The PL peak (~777 nm) appears a slight red shift to the band edge, indicating a small vibrionic relaxation. The time-resolved photoluminescence (TRPL) spectra were obtained on Edinburgh Analytical Instruments F900 with a resolution of 100 ps. Bi-exponential fits were performed to quantify the carrier dynamics. As shown in Fig. S7, the lifetime of the bare material is around 34.3 ns. From which we obtained a fast and a slow time constant of t_1=0.79 ns and t_2=39.19 ns, we associate these two different time scales with the bulk and surface recombination.

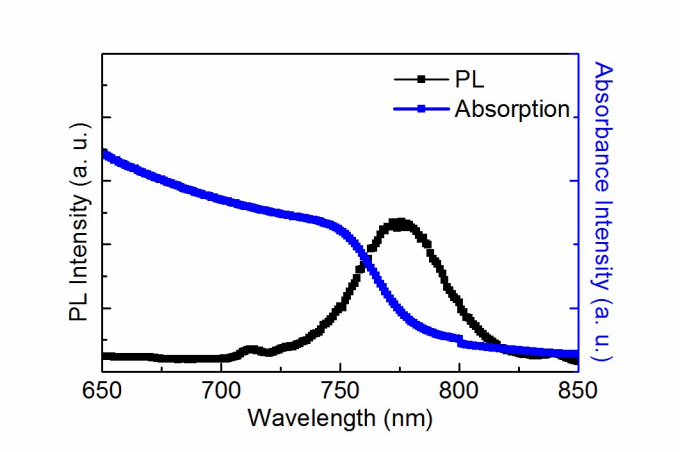

Fig. S6. Steady-state PL and absorbance spectra of the bare $CH_3NH_3PbI_3$ materials.

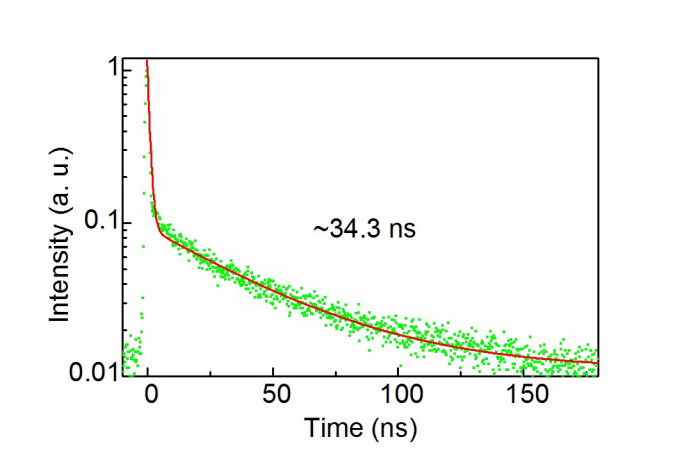

Fig. S7. TRPL decay kinetic of the bare $CH_3NH_3PbI_3$ materials.

5. Optical characterizations of plasmonic $CH_3NH_3PbI_3$ nanowire lasers

To form plasmonic nanowire laser configuration, we chose Ag as the metal due to its low loss and MgF_2 as the gap layer due to its robust property. 100 nm-thick Ag film and 10 nm-thick MgF_2 film were deposited on a silicon substrate by a thermal evaporator continuously. Then $CH_3NH_3PbI_3$ nanowires were dry-transferred onto the sample surface. All of the laser characterization experiments were performed in ambient environment.

The 400 nm pump light was generated from a second harmonic of fundamental input laser (Spectra-Physics, Ti: sapphire-based regenerative laser amplifier system, which generates a linearly-polarized, 800 nm central wavelength beam, with pulse duration of 120 fs and a repetition rate of 1 kHz, seeded by a Spectra-Physics Maitai oscillator). Due to the low repetition rate here, we could avoid the heating problem during the pump process. We changed the polarization of the excitation light to be circular in order to avoid the absorption anisotropy of the nanowires. An objective lens (40×, 0.65 NA) and a cylindrical lens (f=500mm) were used to form an elliptical beam to completely cover a single nanowire. The emission of each nanowire was focused into a spectrograph (Princeton Instruments, Acton SP2300i) with a 300 mm^{-1} grating and a liquid-N_2-cooled charge-coupled device (CCD) (Princeton Instruments, Pylon camera). A Glan-Laser Calcite Polarizer was placed before the

spectrograph slit to analyze the emission polarization of the emitted light. The temperature-dependent spectra were collected by heating the sample with a polyimide heating film which was supplied by a direct-current power, the temperature of the sample was measured by a surface mount thermoelectric couple which was mounted directly on the stage surface, the experiment was conducted after the sample was heated up for at least 30 minutes to reach thermal equilibrium.

The TRPL spectra of an individual plasmonic nanowire laser were investigated with an ultrafast gated camera (Lavision, Picostar HR 12), which was synchronized with the pump laser system by a programmable delay device, which gave us a time resolution of 50 ps.

6. Cavity mode spacing variation versus nanowire length

Shown as in Fig. S8, the mode spacing $\Delta\lambda$ has an approximately linear relationship with inverse nanowire length, which is consistent with a Fabry-Pérot cavity behavior. From the linear fitting line and using $n_g = \lambda^2 / 2\Delta\lambda L$, an average group index of about 9 is estimated.

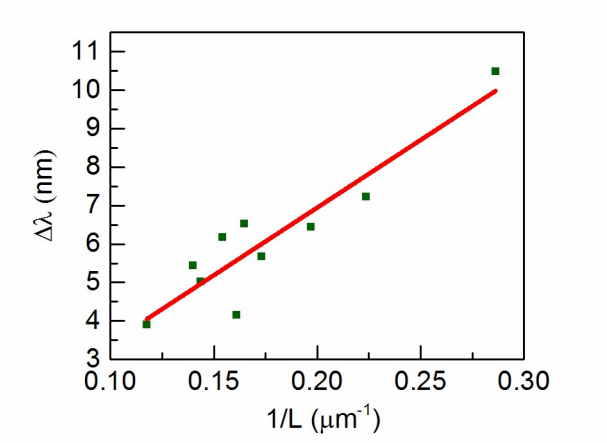

Fig. S8. Mode spacing versus inverse nanowire length.

7. Purcell factor estimation

The local Purcell factor of the fundamental mode is calculated by a similar procedure reported previously.[2] The Purcell factor for a dipole emitter at position r_d within the nanowire with an orientation along the μ direction is approximately,

$$F_\mu(r_d) = \frac{\tau_0}{\tau} \approx 1 + F_{sp,\mu}(r_d) + F_{LSW,\mu} \qquad \text{* MERGEFORMAT (1)}$$

Where $F_{sp,\mu}(r_d)$ is the SPP enhanced emission rate and $F_{LSW,\mu}$ is the lossy surface waves contribution.

$$F_{sp,\mu}(r_d) = \frac{3}{\pi}\frac{n_g}{n_s}\frac{(\lambda/2n_s)^2}{A_{sp,\mu}(r_d)} \qquad \text{* MERGEFORMAT (2)}$$

Where n_g is the SPP mode group index, n_s is the nanowire refractive index. $A_{sp,\mu}(r_d)$ is a measure of mode area for a given dipole orientation and position,

$$A_{sp,\mu}(r_d) = \frac{\int_A W(r)\,\mathrm{d}A}{n(r_d)^2 \varepsilon_0 \left|E_{\mu,sp}(r_d)\right|^2} \qquad \text{* MERGEFORMAT (3)}$$

$W(r)$ is the energy density per unit length along the direction of propagation, given by

$$W(r) = \frac{1}{2}\left[\mathrm{Re}\left\{d(\varepsilon(r)\omega)/\mathrm{d}\omega\right\}\left|E(r)\right|^2 + \mu_0\left|H(r)\right|^2\right] \qquad \text{* MERGEFORMAT (4)}$$

Lossy surface waves are associated with high in-plane momentum leaky waves and are extremely localized,

$$F_{LSW} = \frac{\mathrm{Im}\{\varepsilon_m\}\varepsilon_s}{4\left|\varepsilon_m + \varepsilon_s\right|}\left(\frac{1}{(n_s k_0 h)^3} + \frac{1}{(n_s k_0 h)}\right) + \frac{\mathrm{Im}\{\varepsilon_m\}}{16(n_s k_0 h)} \qquad \text{* MERGEFORMAT (5)}$$

The local Purcell factor distribution is shown in Fig. S9, which has a maximum value of 8.3.

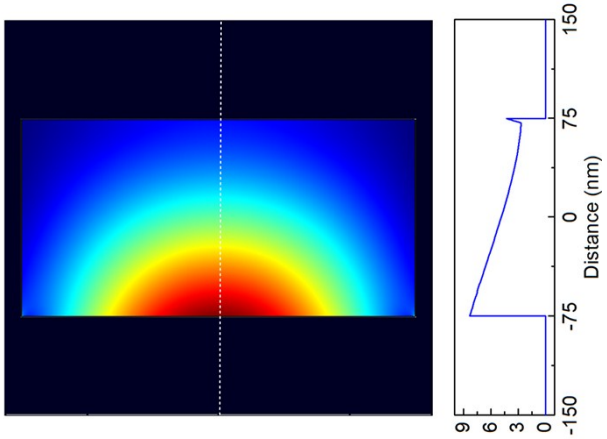

Fig. S9. Calculated local Purcell factor distribution of surface plasmon mode. Cross-sectional Purcell facto plot is shown on the right side. The size of the nanowire is set to be 300 nm × 150 nm, and the thickness of MgF_2 layer is 10 nm.

8. Rate equation analysis

We used a simple rate equation to describe the dynamic evolution of the exciton and surface plasmon density in the plasmonic nanowire laser.[2, 3]

$$\frac{dn}{dt} = \sigma p - An - \Gamma As(\mathrm{n} - \mathrm{n}_0) \qquad \backslash\text{* MERGEFORMAT (6)}$$

$$\frac{ds}{dt} = \beta An + \Gamma As(\mathrm{n} - \mathrm{n}_0) - \gamma \mathrm{s} \qquad \backslash\text{* MERGEFORMAT (7)}$$

Where n is the exciton number, s is the photon number. $p(t) = p_0 \exp(-(t - t_0)^2 / \Delta t^2)$ is the incident pump laser, with a pulse width Δt = 120 fs. n_0 is the exciton number when the gain medium is transparent, which we set to be $\mathrm{volume}_{\mathrm{nanowire}} \times 3 \times 10^{18}$ cm^{-3}.[4] σ is the pump photon to laser photon conversion efficiency. The gain overlap factor $\Gamma \approx 0.6$, which is obtained from finite-element method. A is the average spontaneous emission rate $A = FA_0$, F = 8.3 as calculated previously. A_0 = (4.5 ns)$^{-1}$is the carrier decay rate in bulk $CH_3NH_3PbI_3$.[1] β is the emission coupling factor, which is set to be 0.4 as obtained from the experimental result. The photon lifetime γ can be calculated by,

$$\gamma = (\alpha - \frac{2}{L} \ln R) \upsilon \qquad \backslash\text{* MERGEFORMAT (8)}$$

Where the propagation losses α is 1190 cm^{-1} for the data of Johnson & Christy,[5] L=6 μm as estimated from experiments, R is the nanowire facet reflectivity which we assume to be 0.2

for simplification, and υ is the group velocity of the mode. Using the above method, the carrier density at threshold is estimated to be $\sim 3\times 10^{18} cm^{-3}$.

9. Emission polarization of the plasmonic $CH_3NH_3PbI_3$ nanowire laser

We performed a complete polarization analysis over 360 degrees with an interval of 30 degrees for a representative nanowire. Shown as in Fig. S10, the emission polarization is highly parallel to the nanowire axis, which further substantiates the lasing is from the plasmon modes.

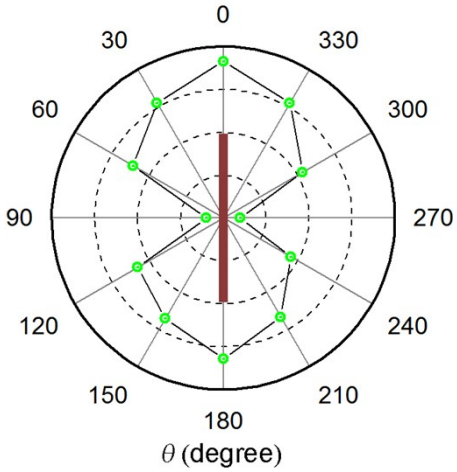

Fig. S10. The polar plot of the emission intensity

10. Dimension characterizations of plasmonic $CH_3NH_3PbI_3$ nanowire lasers

In order to analyze the dimension of those nanowires that supported plasmonic lasing, we conducted SEM characterization to measure the length and the width of the nanowires, and atomic force microscope (AFM, Bruker ICON) to measure the height of the nanowires after the optical characterization. For width and length analysis, each nanowire was sampled 10 positions to give an average value. Fig. S11 shows SEM and AFM images of a nanowire which was lasing in photonic mode (length 5.65 μm, average width 304 nm, average height 430 nm). Fig. S12 shows the threshold performance against the related nanowires' height, the smallest height we measured here is 108.9 nm. Fig. 13 shows the measured central emission

wavelength of the plasmonic nanolasers against the height at around 3 ~ 4 times of the threshold pump power. The Plasmonic devices investigated here lase from 767.76 nm to 796.75 nm. Fig. S14 shows SEM image and AFM image of a representative plasmonic nanowire (length 5.135 μm, average width 126 nm, average height 169 nm). Fig. 15 shows the mode simulation and the lasing spectra for the smallest lasing nanowires.

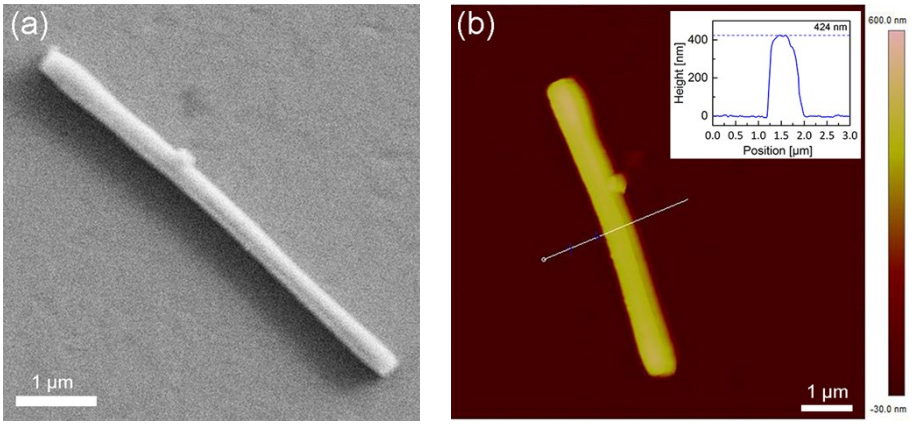

Fig. S11. Dimension measurements of a $CH_3NH_3PbI_3$ nanowire which was lasing in photonic mode. (a) The SEM showing the nanowire has an average width of 304 nm and a length of 5.65 μm. (b) The AFM image showing the nanowire has an average height of 430 nm. Inset: A cutline profile of the nanowire with a height of 424 nm.

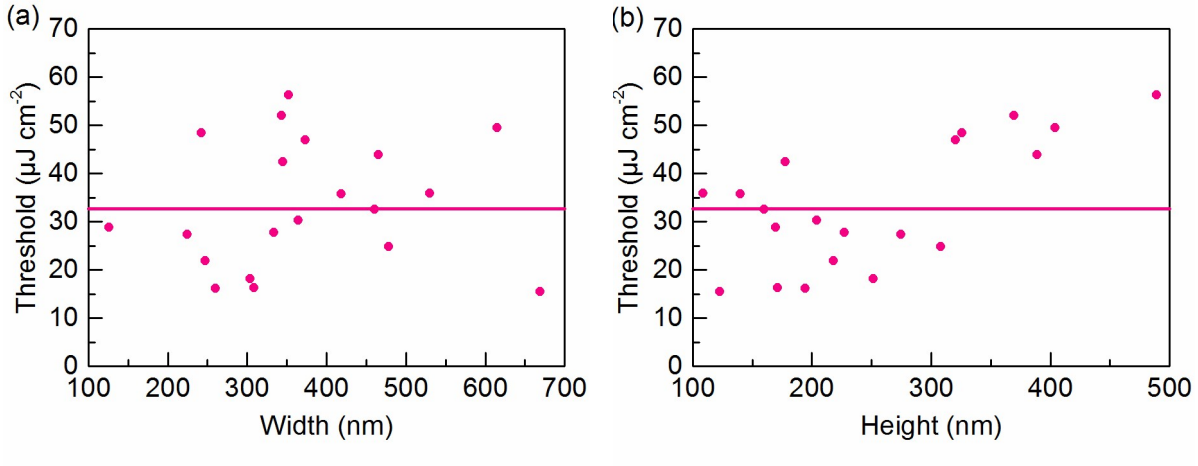

Fig. S12. Threshold performance with the related heights of nanowires.

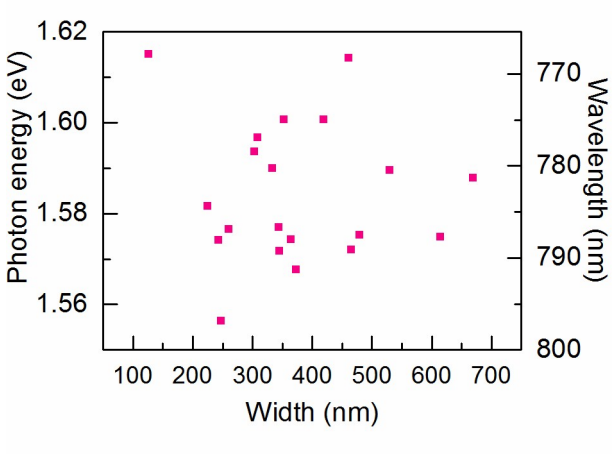

Fig. S13. Measured central emission wavelength of the plasmonic nanolasers against the height at around 3 ~ 4 times of the threshold pump power. The Plasmonic devices investigated here lase from 767.76 nm to 796.75 nm with more than half of the nanowires lasing below 787 nm.

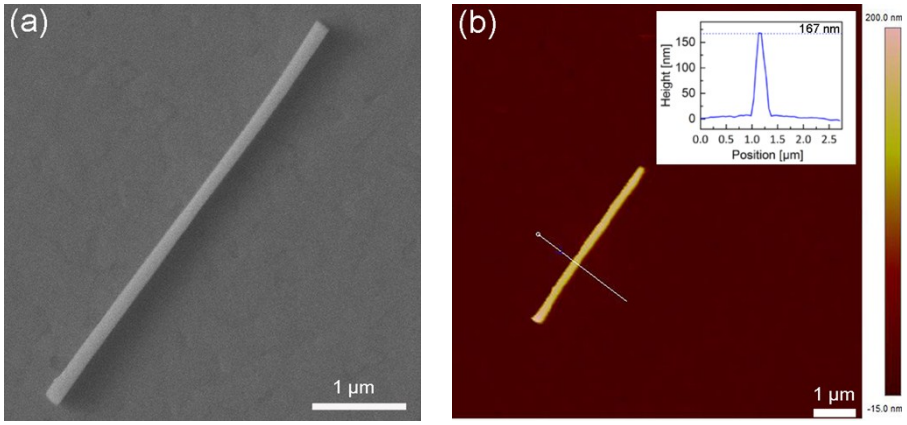

Fig. S14. Dimension measurements of a $CH_3NH_3PbI_3$ nanowire. (a) The SEM image showing the nanowire with an average width of 126 nm and a length of 5.135 μm. (b) The AFM image showing the nanowire with an average height of 169 nm. Inset: A cutline profile of the nanowire with a height of 167 nm.

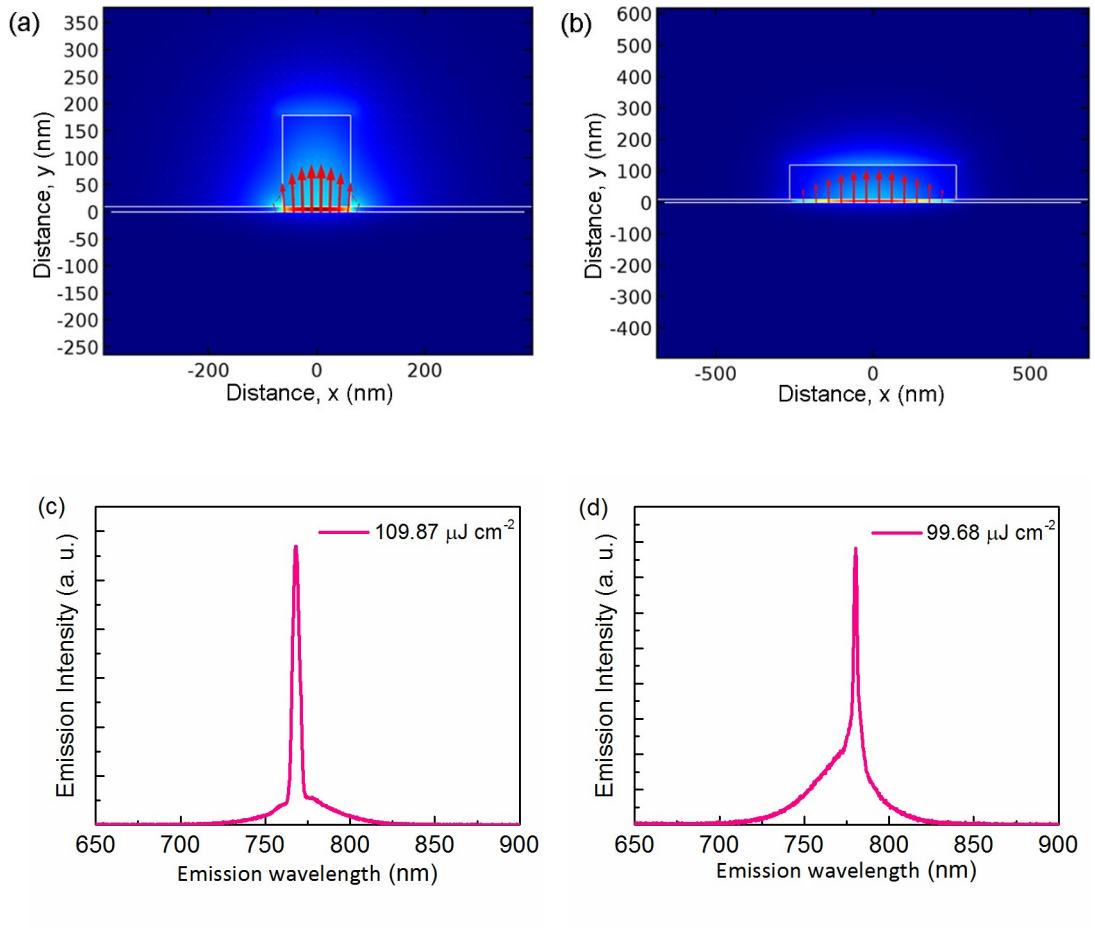

Fig. S15. Calculated mode distributions and lasing spectrum for nanowires: (a), (c) 126 nm × 169 nm, (b), (d) 530 nm × 109 nm. The red arrows indicate the electric field direction.

11. TRPL decay kinetics of photonic $CH_3NH_3PbI_3$ nanowire laser

$CH_3NH_3PbI_3$ nanowires were dry transferred on to a silicon substrate which has 300 nm oxidized layer on top. Then the TRPL measurement of a photonic laser was performed. Biexponential decay function was used to fit the TRPL decays. Shown as in Fig. S16, the SPE lifetime is τ_{SPE} = 2.42 ns at low pump densities (P ~ 0.25P_{th}), and decreases to 1.46 ns when the pump density was increased to around the threshold. Once the pump power is above the threshold, the lifetime is further decreased (τ_{lasing}≤50 ps, instrument limited).

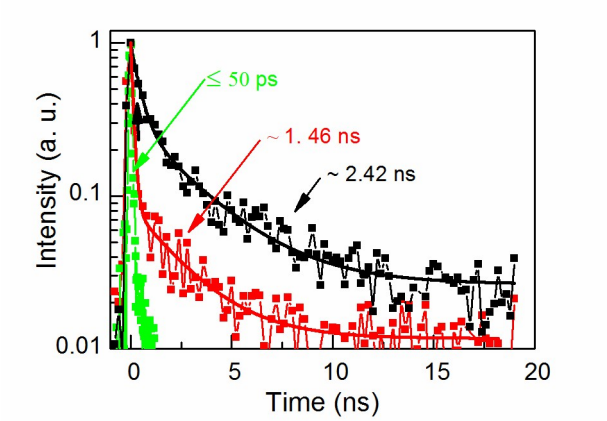

Fig. S16. TRPL decay kinetics of a photonic $CH_3NH_3PbI_3$ nanowire laser

12. Phase confirmation at 43.6 °C

We performed XRD measurement for our samples at 43.6°C to confirm the phase state, as shown in Fig. S17 the diffraction patterns are almost the same with those of the room temperature (RT) samples.

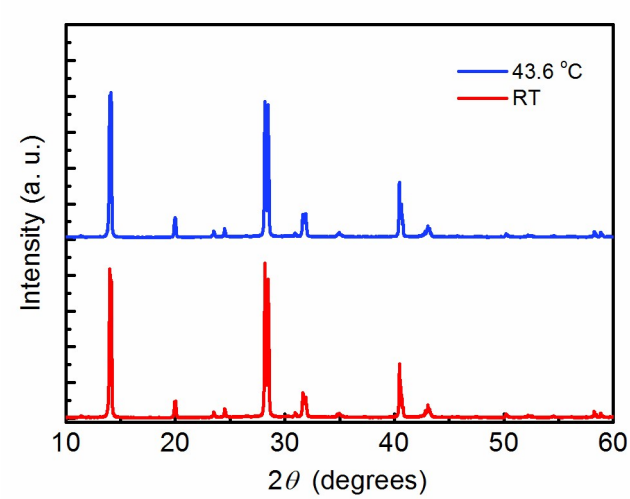

Fig. S17. XRD diffraction patterns at room temperature and 43.6°C

13. Stability of perovskites under illumination

To test the stability of our samples at high excitation densities, we illuminated the as-grown sample for 15 minutes with a density of 255 μJ/cm2, which is 5 times of the maximum threshold of our plasmonic lasers, then we performed XRD measurement. The XRD

diffraction patterns are shown in Fig. S18, the illumined sample and the as-grown sample show the same diffraction patterns, illustrating that the sample is stable under such high illumination.

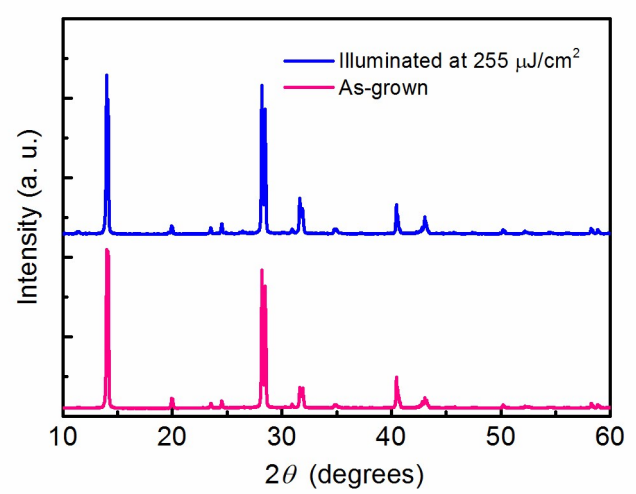

Fig. S18. XRD diffraction patterns for as-grown sample and illuminated sample

References

1. G. Xing, N. Mathews, S. S. Lim, N. Yantara, X. Liu, D. Sabba, M. Gratzel, S. Mhaisalkar and T. C. Sum, *Nat. Mater.*, 2014, **13**, 476-480.
2. R. F. Oulton, V. J. Sorger, T. Zentgraf, R.-M. Ma, C. Gladden, L. Dai, G. Bartal and X. Zhang, *Nature*, 2009, **461**, 629-632.
3. H. Yokoyama and S. D. Brorson, *Journal of Applied Physics*, 1989, **66**, 4801.
4. I. Suárez, E. J. Juárez-Pérez, J. Bisquert, I. Mora-Seró and J. P. Martínez-Pastor, *Adv. Mater.*, 2015, **27**, 6157-6162.
5. P. B. Johnson and R.-W. Christy, *Phys Rev B*, 1972, **6**, 4370.